Proceedings of ISFOG 2025
5TH INTERNATIONAL SYMPOSIUM ON
FRONTIERS IN OFFSHORE GEOTECHNICS
Nantes, France | June 9-13 2025

ISBN 978-2-85782-758-0

Numerical Simulation of a Model Monopile Test for Large Offshore Wind Turbine Subjected to Cyclic Loading

M. F. Erener*
Ege University, Izmir, Türkiye

C. T. Akdag
Technische Universität Berlin, Berlin, Germany

D. S. Erdogan
Ege University, Izmir, Türkiye

T. Tufan Erener
Ege University, Izmir, Türkiye

**fahrettinerener@gmail.com (corresponding author)*

ABSTRACT: Experimental and numerical studies play a crucial role in the studies of understanding the long-term behavior of offshore wind turbines (OWTs) with monopile foundation under cyclic loading conditions. In this study, numerical simulations of a model test, which corresponded to a 9-meter-diameter prototype monopile foundation for an OWT with an 8 MW capacity, were performed using OpenSeesPL. Pressure Dependent Multi-Yield Surface Plasticity Model (PDMY) was used to represent undrained soil behavior of sand. The effects of mesh size and the soil backbone curve on the pile response were assessed under cyclic loading conditions. It was observed that soil elements with backbone curves at low mean effective stress levels showed better agreement with test results in terms of pile displacements and rotations around pile head level due to lower effective stresses in this region. The study showed that mesh size and backbone curve characteristics were interrelated in determining the lateral pile response.

Keywords: Offshore wind turbine; Monopile; OpenSees; Pressure Dependent Multi-Yield (PDMY); Numerical simulation

1 INTRODUCTION

Offshore wind turbines (OWTs) have seen rapid advancements in recent years, with energy production capacities reaching up to 10 MW. Turbine components with large sizes, such as blades and towers, are required to accommodate substantial energy production. This allows wind speeds suitable for such production to be accessed at altitudes of nearly 100 meters above sea level or higher. In addition to altitude, these wind speeds are found at specific distances from the shore. Under these conditions, monopile foundations provide a practical and widely adopted solution in foundation engineering. A simple schematic representation of these structures is shown in Figure 1.

The behavior of OWT monopile foundations has been investigated through both experimental and numerical approaches. These studies play a crucial role in understanding the behavior of the foundations of OWTs. Several experimental studies have been conducted to enhance the understanding of the behavior of monopile foundations for OWTs. One notable effort in these studies is the Pile Soil Analysis (PISA) project, which aimed to develop an improved design methodology for laterally loaded monopiles. The project involved both medium-scale field tests and numerical analyses. A total number of 28 field tests were conducted on monopiles with diameters of up to 2 meters. The results of the study showed that the accuracy in predicting lateral soil reaction was improved by p-y curves developed in the PISA project (Byrne et al., 2015; Byrne et al., 2017).

With regard to the investigation of monopile behavior under cyclic loading, several studies including model tests have been published in recent literature. Rudolph et al. (2014) conducted centrifuge model tests under field-representative stress conditions at 200g, revealing that loading direction significantly influences the accumulation of pile head displacement. Nanda et al. (2017) performed 1g small-scale model tests in dense sand and observed greater lateral displacements and reduced lateral pile stiffness under multidirectional cyclic loading compared to unidirectional loading.

In addition to experimental studies, numerous numerical investigations have been conducted (Achmus et al., 2009; Barari et al., 2017; Liu and

Kaynia, 2023), including 3D finite element simulations to examine monopile behavior. The use of advanced computational techniques enables the simulation of the behavior of OWTs with monopile foundations and the surrounding soil under cyclic loading conditions. However, for numerical models to yield reliable results, they must accurately represent the actual behavior of the prototype. It is worth noting that the accuracy and reliability of numerical models can be ensured through calibration using data obtained from experimental studies.

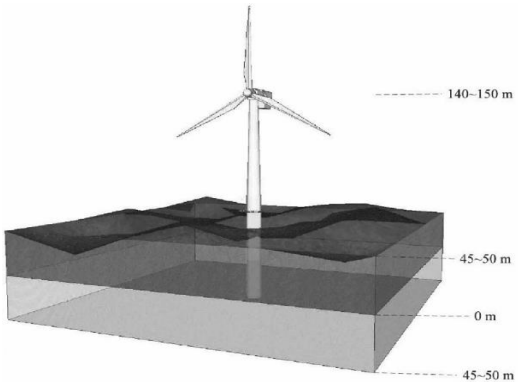

Figure 1. Sketch of a large OWT with monopile foundation (Akdag et al., 2023).

In this study, the effects of both mesh size and the selection of stiffness properties on the results of numerical simulations were investigated for a model test conducted by Akdag et al. (2023). Four different cases were considered in the numerical models comprising combination of two mesh sizes and two stiffness conditions. The numerical simulation of the small-scale model test was performed using OpenSeesPL software. An advanced constitutive soil model, PDMY (Pressure Dependent Multi-Yield Surface Plasticity), was used to represent the undrained behavior of sand under cyclic loading conditions. Below, a brief assessment of modelling issues and their consequences on the analysis results is presented.

2 METHODOLOGY

In this section, the model test setup used in numerical analyses is described. Subsequently, key features of the constitutive model are presented. Finally, the numerical model is introduced in terms of dimensions and element properties for both the soil and the pile. The different numerical model cases to be investigated are outlined with respect to mesh size and stiffness properties.

2.1 Model Test

The small scale model test considered for the numerical simulation in this study was conducted by Akdag et al. (2023) and represented a 9-meter-diameter prototype monopile foundation of an OWT with an 8 MW capacity. The embedment length of the prototype monopile was 50 meters, and the length-to-diameter ratio was L/D = 5.55. The model test consisted of a steel monopile with an outer diameter of D = 20 cm and an embedment length of L = 3.20 m, installed in saturated medium dense sand. Wall thickness of the tubular pipe pile was $t = 3.0$ mm. Dimensions of test pit containing the sand were 4.00 m (longitudinal), 3.00 m (transverse) and 3.80 m (vertical). In the test, a total of 12,000 cycles were applied at the pile head as unidirectional lateral sinusoidal cyclic loading with a frequency of f = 0.20 Hz. Amplitude of horizontal load was $H_{\max}$ = 15 kN which corresponded to approximately 15% of the ultimate lateral load capacity of model test pile (Akdag et al., 2023). A cross-section of testing system is shown in Figure 2. The index and mechanical properties of Cottbuser Sand, which was used in the experiment, are given in Table 1.

Table 1. Properties of Cottbuser Sand (Akdag et al., 2023).

Property	Symbol	Unit	Value
Max. void ratio	$e_{\max}$	-	0.82
Min. void ratio	$e_{\min}$	-	0.50
Average void ratio	e	-	0.62
Dry density	ρ_{d}	g/cm^3	1.64
Relative density	D_{R}	-	0.64
Friction angle	ϕ'	Degrees	41.60°

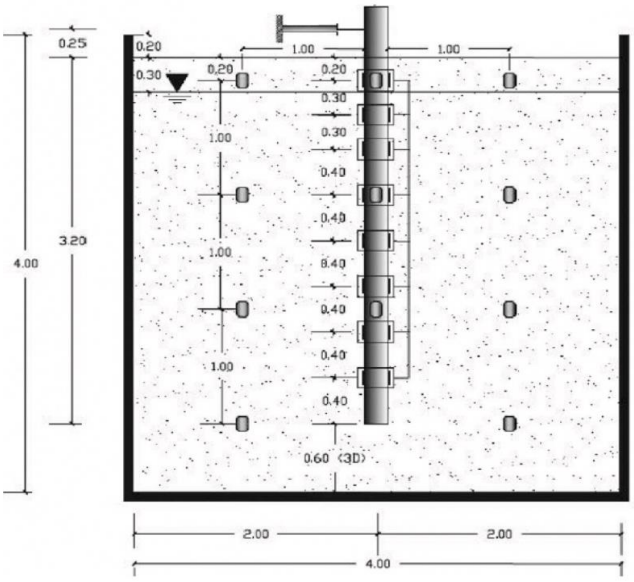

Figure 2. Cross section of testing system (reproduced from Akdag et al., 2023).

In the study of Akdag et al. (2023), the scaling considerations of physical dimensions (Wood, 2004) and the behavior of the pile under lateral loading, which can change from rigid to flexible (Davisson, 1970; Poulos, 1982; Abadie et al., 2019), were considered. It was concluded that the response of the scaled model pile could represent the behavior of the prototype monopile. The details of the scaling relations can be found in the studies Akdag et al. (2023) and Akdag and Rackwitz (2023).

In this test, pile head displacement accumulation resulting from lateral loading was measured using displacement transducers installed on the pile head and strain development was acquired by strain gauges installed along the pile length.

2.2 Constitutive Soil Model

As part of this study, three-dimensional finite element computations were performed using OpenSeesPL software. This software uses OpenSees (Open System for Earthquake Engineering Simulation), an open-source software framework developed for simulations of both structural and geotechnical problems under dynamic loading conditions (Mazzoni et al., 2006).

An advanced constitutive model, PDMY (Pressure Dependent Multi-Yield Surface Plasticity), was selected in numerical modelling to represent the undrained behavior of sand under cyclic loading conditions. PDMY is capable of simulating nonlinear soil behavior under both cyclic and seismic loading conditions. It is one of the advanced constitutive models capable of simulating cyclic mobility behavior. Model considers controlling the magnitude of cycle-by-cycle permanent shear strain accumulation (Yang et al., 2003). Also, cyclic mobility mechanism is represented by loading-unloading flow rules reproducing dilation tendency.

Material response under monotonic or cyclic loading can be simulated by shear behavior with pressure dependency. The ability of the material model to account for the effective confinement in yield behavior and plastic flow enhances the response under varying stress levels.

One of the distinguishing features of the constitutive model is the representation of nonlinear stress-strain behavior which is represented with a hyperbolic backbone curve (Kondner, 1963) (Figure 3). Backbone curves based on effective confinement levels enables the model to construct yield surfaces (Figure 4).

2.3 Numerical Model

Four finite element (FE) models were established in OpenSeesPL, using different mesh sizes and soil backbone curves to evaluate the effect of meshing and stiffness properties on the monopile response under cyclic loading conditions. In terms of mesh size, two assumptions were made. Here, mesh sizes in vertical direction (l_z) along depth were selected as 1/10 and 1/30 of the embedded pile length (L_e). Considering small scale effect, two different reference vertical effective stress levels ($(\sigma'_v)_{ref}$ = 20 kPa and $(\sigma'_v)_{ref}$ = 100 kPa) were selected to investigate the influence of pressure dependency on nonlinear soil behavior. All model cases are summarized in Table 2.

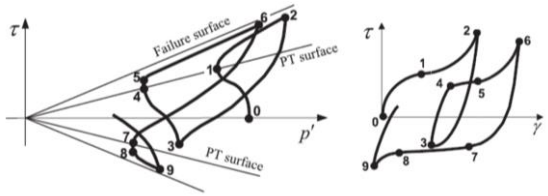

Figure 3. Stress path and shear stress-shear strain relationship (reproduced from Khosravifar et al., 2018).

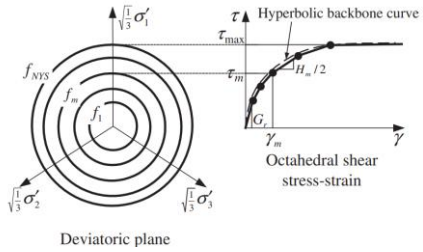

Figure 4. Backbone curve and yield surfaces (Yang and Elgamal, 2003).

Table 2. Different model cases considered in this study.

Property	Unit	Case 1	Case 2	Case 3	Case 4
$(\sigma'_v)_{ref}$	kPa	20	20	100	100
l_z/L_e	-	1/10	1/30	1/10	1/30

2.3.1 General information and mesh size

Numerical models were established in OpenSeesPL. Eight-node hexahedral linear isoparametric *u-p* elements (BrickUP) were used to represent soil-fluid coupled material. *u-p* elements are derived from Biot formulations in which deformation of soil skeleton and the flow of pore fluid are represented by two separate differential equations and they are solved in coupled form.

Mesh sizes in vertical direction (Z) were determined as 1/10 (32 cm) and 1/30 (10.67 cm) of the embedded pile length for different numerical model cases considered in this study. In these models, mesh sizes in longitudinal (X) and transverse (Y) directions were adjusted by the software to provide a mesh that becomes finer from the outer boundaries of the model toward the center (Figure 5). Since the lateral loading is unidirectional and the system is axisymmetric, only half of the model test system was modeled.

The pile element was modeled with beam and rigid link elements. Nodes at each end of a beam element were connected to the nodes corresponding to physical locations of outer boundary of tubular pile section. This allowed different soil responses inside and outside the pile zone to be obtained.

In this study, only the first 100 cycles of lateral cyclic loading were simulated. The pushover load defined as a sinusoidal load with a 5-second cycle period, corresponding to a total simulation time of 500 seconds.

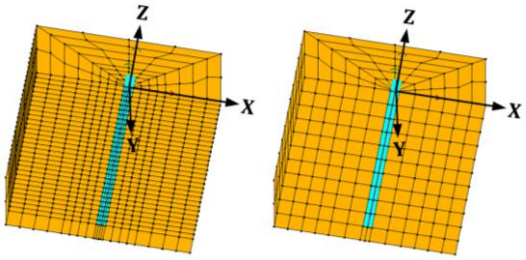

Figure 5. Numerical models with different mesh sizes.

2.3.2 Pile and soil properties

Material behavior for pile under the cyclic loading in the model test was assumed to be linear elastic. Therefore, steel material is represented by a linear elastic material in numerical model. Elastic modulus, shear modulus and Poisson's ratio of steel is E=210 GPa, G=80.77 GPa and υ=0.30, respectively.

Internal friction angle of soil was obtained as ϕ'=41.6° from the direct shear tests carried out by Akdag et al. (2023). The constitutive soil model uses an internal friction angle corresponding to triaxial compression test. According to a literature review by Lini Dev et al., (2016), direct shear angle is typically 2°~8° higher than that from triaxial compression test for sands. Considering an average value of ~6° degrees, the triaxial compression angle was assumed ϕ_{TXC} =36° in numerical simulations. The relationship between triaxial compression friction angle (ϕ_{TXC}) and the direct simple shear (DSS) friction angle (ϕ_{DSS}) can be obtained using Equation 1 (Khosravifar, 2012). Poisson's ratio (υ) of soil was calculated using Equation 2 (Federico and Elia, 2009).

The low-strain shear modulus ($G_{\max}$) and low-strain bulk modulus ($B_{\max}$) of the soil at any reference vertical effective stress can be calculated in kPa units, based on the index properties of the soil. First, the equivalent overburden corrected SPT-N value ($N_{1,60}$) is calculated using relative density and void ratio values through Equation 3 (Ghali et al., 2020). Here, C_{D} represents the normalized blow counts factor. Then, shear wave velocity at reference vertical effective stress of $\sigma_{\mathrm{v}}^{'}$ =100 kPa (V_{S1}) is calculated in m/s units using Equation 4 (Andrus and Stokoe, 2000).

By incorporating the pressure dependency law into well-known shear modulus-shear wave velocity relationship, $G_{\max}$ and $B_{\max}$ at any reference vertical effective stress level can be computed using Equation 5 and Equation 6, respectively. In these equations, the parameter m represents the pressure dependency coefficient. The relationship between the reference effective vertical stress ($(\sigma_{\mathrm{v}}')_{\mathrm{ref}}$) and the reference mean effective stress ($(p')_{\mathrm{ref}}$) is given in Equation 7. Units for all stress and density values in the above equations expressed in kPa and t/m^3, respectively.

$$\phi_{\mathrm{TXC}} = \sin^{-1}\left[\frac{3\tan(\phi_{\mathrm{DSS}})}{2\sqrt{3}+\tan(\phi_{\mathrm{DSS}})}\right] \quad (1)$$

$$\upsilon = \frac{1-\sin(\phi_{\mathrm{TXC}})}{2-\sin(\phi_{\mathrm{TXC}})} \quad (2)$$

$$C_D = \frac{N_{1,60}}{{D_R}^2} = \frac{16.5}{(e_{max}-e_{min})^{1.5}} \quad (3)$$

$$V_{S1} = 93.2(N_{1,60})^{0.231} \quad (4)$$

$$G_{max} = \rho(V_{S1})^2\left[\frac{(\sigma_v')_{ref}}{100}\right]^m \quad (5)$$

$$B_{max} = G_{max}\left(\frac{2+2\upsilon}{3-6\upsilon}\right) \quad (6)$$

$$(p')_{ref} = (\sigma_v')_{ref}\left[\frac{3-2\,sin(\varphi_{TXC})}{3}\right] \quad (7)$$

Typical values of cohesion (c), combined bulk modulus (K), peak octahedral shear strain ($\gamma_{\max}$), permeability (k), phase transformation angle (ϕ_{PT}), and saturated mass density (ρ_{sat}) of sand were obtained from Lu et al. (2011). The material properties used in the simulations are summarized in 3.

The parameters defined in the constitutive model represent soil properties at the reference mean effective stress. The pressure dependency law enables the model to construct stress-strain relationships at any mean effective stress level. Typically, reference vertical effective stress level at which soil parameters are defined is taken as $(\sigma_{\mathrm{v}}')_{\mathrm{ref}}$ = 100 kPa or $(\sigma_{\mathrm{v}}')_{\mathrm{ref}} \cong$ 1 atm. In this study, however, the average vertical effective stress in the soil medium, $(\sigma_{\mathrm{v}}')_{\mathrm{ave}}$ = 20 kPa, was used as the reference vertical effective stress. Accordingly, both the influence and the suitability of selecting this reference vertical effective stress on soil backbone curve, as well as model's ability to construct nonlinear stress-strain relationships under different effective stresses, were evaluated.

Table 3. Soil properties for all model cases.

Property	Unit	Cases 1&2	Cases 3&4
ρ_{sat}	g/cm^3	1.92	1.92
$(\sigma'_v)_{ref}$	kPa	20	100
$(p')_{ref}$	kPa	12	61
m	-	0.5	0.5
G_{max}	MPa	39.0	88.0
B_{max}	MPa	80.7	182.0
γ_{max}	%	10	10
ϕ_{TXC}	Degrees	36	36
ϕ_{PT}	Degrees	27	27
c	kPa	1	1
K	GPa	2.2	2.2
k	m/s	6.6E-05	6.6E-05
v	-	0.29	0.29
C_D	-	91	91
V_{S1}	m/s	215	215
$N_{1,60}$	Blows/ft	37.3	37.3

Using different reference vertical effective stresses, the backbone curves and soil model responses of a single element under undrained monotonic loading in DSS conditions are given in Figure 6 and, Figure 7 respectively. In Figure 6, the backbone curves and shear modulus reduction curves indicate that the single element corresponding to lower reference mean effective stresses exhibits a softer response, starting from approximately $\gamma_{xy} \geq 10^{-5}$. This corresponds to the small shear strain level, when small deformations are observed at the pile head due to cyclic loading. The difference between the two shear modulus reduction curves is anticipated to be a significant factor affecting the lateral soil response and pile behavior during the initial cycles of cyclic loading.

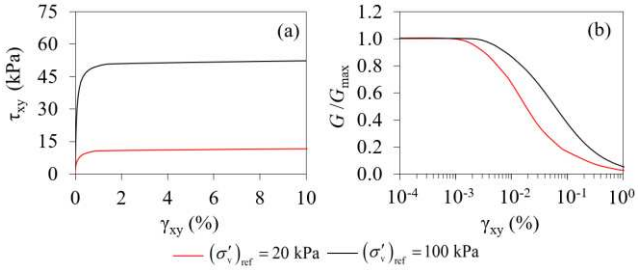

Figure 6. Backbone curves (a) and shear modulus reduction curves (b) for different reference vertical effective stress levels.

Figure 7 shows stress-strain and undrained effective stress path responses of a single element under DSS conditions. It is clear from these figures that single simple shear elements for both $(\sigma'_v)_{ref}$ = 100 kPa and $(\sigma'_v)_{ref}$ = 20 kPa exhibit dilative tendency under undrained monotonic loading conditions. This behavior is consistent with the undrained shear strength behavior of medium dense sand. Dilative tendency observed in these figures is the result of decrease in excess pore water pressures during straining. Accordingly, dilative tendency causes strain hardening stress strain behavior. This is evident from the undrained effective stress paths, all of which ascend along the critical state line of the soil element. It is also apparent that samples under lower effective stresses tend to dilate under smaller shear strain levels, which is expected.

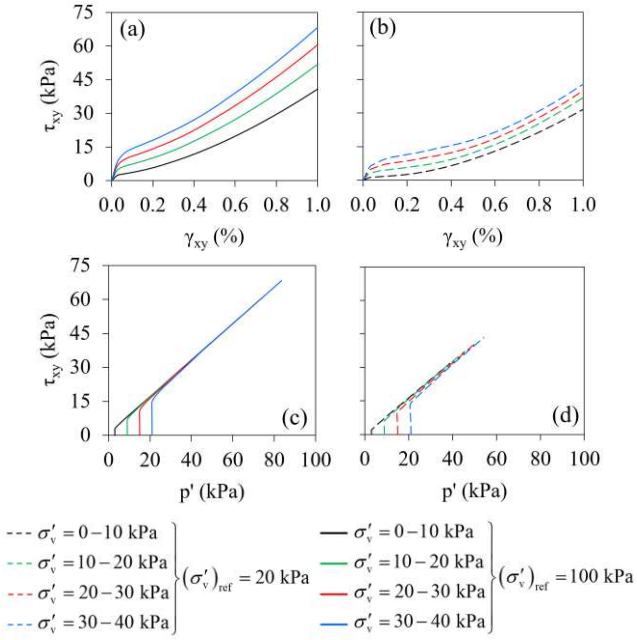

Figure 7. Simulation of undrained monotonic DSS test on single element using $(\sigma'_v)_{ref}$=20 kPa and $(\sigma'_v)_{ref}$=100 kPa. Stress-strain responses (a and b) and stress paths (c and d) at varying effective stresses.

3 RESULTS

Four numerical analyses were conducted, considering combinations of different reference vertical effective stresses and mesh sizes (Table 2). The results from both the numerical simulations and the model test at the 1st, 40th, and 80th cycles (N) are presented in Figure 8 and Figure 9. For ease of comparison, depths were normalized by pile length, while the displacements were normalized by pile diameter.

Up to ten cycles, pile head displacements in both Case 1 and Case 2 were consistent with the experimental results. In terms of displacement amplitude within a single cycle and mean pile head displacements, there was good agreement between the model test and the simulation results of Case 2, in which a smaller mesh size was used. In contrast, the mean displacements in Case 3 and Case 4 were approximately 1.5 times lower than those observed in the experimental results. Unlike the first 10 cycles, Case 1 appeared more suitable than Case 2. This can

be attributed to the influence of mesh size, which generates small elements with lower effective stress. The corresponding soil response, governed by the backbone curve, results in a softer response at these effective stress levels.

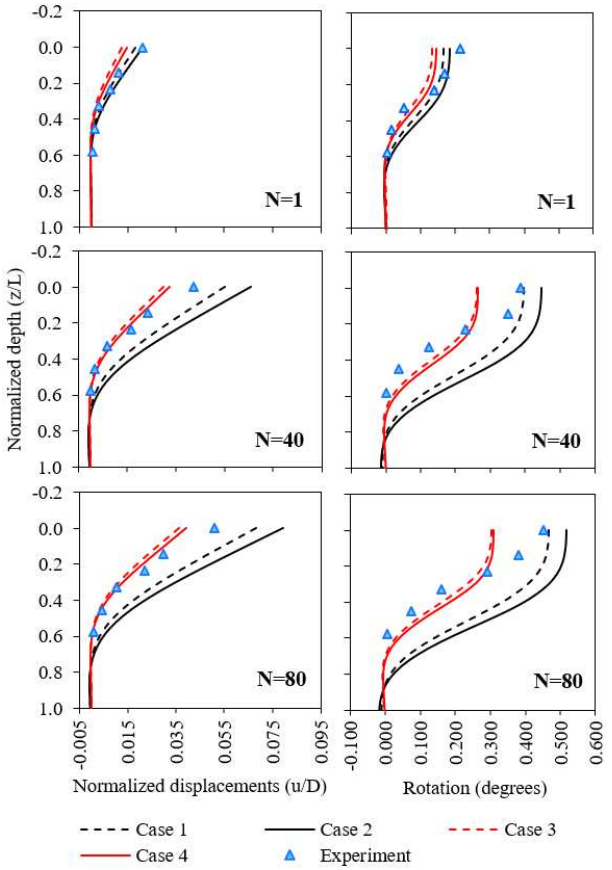

Figure 8. Normalized displacements and rotations along the pile at the 1st, 40th and 80th cycles.

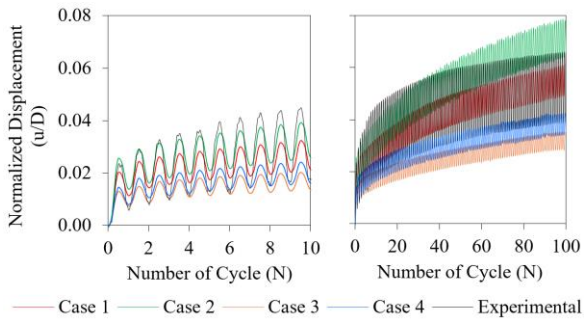

Figure 9. Normalized head displacements up to 10 and 100 cycles.

In terms of pile rotations, Case 1 and Case 2 provided more accurate results at the pile head level for depths where z/L≤0.2. However, beyond these depths, both pile rotations and displacements from Case 3 and Case 4 aligned more closely with experimental results. It was deduced that the soil response modeled with a backbone curve based on $(\sigma'_v)_{ref}$=100 kPa was more suitable for pile behavior at depths where z/L>0.2. While approaching the pile head, in regions with low effective stresses, use of the backbone curve at $(\sigma'_v)_{ref}$=20 kPa yielded more reliable results.

4 CONCLUSIONS

This study was primarily focused on the numerical simulation of a small-scale model test of a large OWT with monopile foundation and the effects of mesh size and backbone curve selection on both soil and pile behavior. It was observed that refining the mesh size led to generation of small solid elements with lower effective stresses where stress-strain response becomes softer due to stress dependency law. In addition, selecting a reference effective stress level for the backbone curve based on average effective stress of the model test pit resulted in better agreement with both pile head displacements and pile head rotations. However, for depths where z/L>0.2, displacements and rotations were obtained accurately through the use of backbone curve with $(\sigma'_v)_{ref}$=100 kPa.

Outcomes of this study revealed that the relationship between mesh size and backbone related soil stress-strain behavior was important in numerical simulation. It should be noted that the conclusions of this study are only valid for the model test considered and under its testing conditions. For future studies, additional numerical simulations of different model tests under varying test conditions should be performed to verify and strengthen the findings.

AUTHOR CONTRIBUTION STATEMENT

Mehmet Fahrettin Erener: Data curation, Software, Methodology, Visualization, Writing- Original draft. **Devrim Sufa Erdogan:** Methodology, Supervision, Writing- Reviewing and Editing. **Cihan Taylan Akdag:** Methodology, Supervision, Writing- Reviewing and Editing. **Tugce Tufan Erener:** Visualization, Writing- Reviewing and Editing.

REFERENCES

Abadie, C. N., Byrne, B. W., & Houlsby, G. T. (2019). Rigid pile response to cyclic lateral loading: Laboratory tests. *Geotechnique*, 69(10), 863–876. https://doi.org/10.1680/jgeot.16.P.325

Achmus, M., Kuo, Y. S., & Abdel-Rahman, K. (2009). Behavior of monopile foundations under cyclic lateral load. *Computers and Geotechnics*, *36*(5), 725-735.https://doi:10.1016/j.compgeo.2008.12.003.

Akdag, C. T., Isik, N., Le, V. H., and Rackwitz, F. (2023). Test results for a monopile in medium dense sand subjected to unidirectional lateral cyclic loading. *European Journal of Environmental and Civil Engineering*, *27*(5), 1957-1988. https://doi.org/10.1080/19648189.2022.2107576

Akdag, C. T., & Rackwitz, F. (2023). Model test and finite element analysis results of a monopile in very dense sand under unidirectional horizontal cyclic loading. *Ocean Engineering*, *288*, 116053. https://doi.org/10.1016/j.oceaneng.2023.116053

Andrus, R. D., and Stokoe, K. H. (2000). Liquefaction resistance of soils from shear-wave velocity. *Journal of geotechnical and geoenvironmental engineering*, *126*(11), 1015-1025. https://doi.org/10.1061/(ASCE)1090-0241(2000)126:11(1015)

Barari, A., Bagheri, M., Rouainia, M., & Ibsen, L. B. (2017). Deformation mechanisms for offshore monopile foundations accounting for cyclic mobility effects. *Soil Dynamics and Earthquake Engineering*, *97*,439-453. https://doi.org/10.1016/j.soildyn.2017.03.008.

Byrne, B. W., Burd, H. J., Zdravković, L., McAdam, R. A., Taborda, D. M., Houlsby, G. T., ... & Gavin, K. G. (2019). PISA: new design methods for offshore wind turbine monopiles. *Revue Française de Géotechnique*, (158), 3.

Byrne, B. W., McAdam, R., Burd, H. J., Houlsby, G. T., Martin, C. M., Zdravkovic, L., ... & Skov Gretlund, J. (2015). New design methods for large diameter piles under lateral loading for offshore wind applications. *Frontiers in offshore geotechnics III*, *1*, 705-710.

Davisson, M. (1970). Lateral load capacity of piles. In *49th Annual Meeting of the Highway Research Board* (pp. 104–110).

Federico, A., & Elia, G. (2009). At-rest earth pressure coefficient and Poisson's ratio in normally consolidated soils. In *Proceedings of the 17th International Conference on Soil Mechanics and Geotechnical Engineering (Volumes 1, 2, 3 and 4)* (pp. 7-10). IOS Press.

Ghali, M., Chekired, M., and Karray, M. (2020). Framework to improve the correlation of SPT-N and geotechnical parameters in sand. *Acta Geotechnica*, *15*, 735-759. https://doi.org/10.1007/s11440-018-0745-3

Khosravifar, A. (2012). *Analysis and design for inelastic structural response of extended pile shaft foundations in laterally spreading ground during earthquakes*, PhD Thesis, University of California, Davis.

Khosravifar, A., Elgamal, A., Lu, J., and Li, J. (2018). A 3D model for earthquake-induced liquefaction triggering and post-liquefaction response. *Soil Dynamics and Earthquake Engineering*, *110*, 43-52. https://doi.org/10.1016/j.soildyn.2018.04.008

Kondner, R. L. (1963). A hyperbolic stress strain formulation for sands. In *Proc. 2nd Pan-American Conf. on SMFE* (Vol. 1, pp. 289-324).

Lini Dev, K., Pillai, R. J., & Robinson, R. G. (2016). Drained angle of internal friction from direct shear and triaxial compression tests. *International Journal of Geotechnical Engineering*, *10*(3), 283-287.

Liu, H., & Kaynia, A. M. (2023). Characteristics of cyclic undrained model SANISAND-MSu and their effects on response of monopiles for offshore wind structures. *Géotechnique*, *73*(4), 294-309. https://doi.org/10.1680/jgeot.21.00068.

Lu, J., Elgamal, A., and Yang, Z. (2011). OpenSeesPL: 3D lateral pile-ground interaction user manual (Beta 1.0). *Department of Structural Engineering, University of California, San Diego*, 147.

Mazzoni, S., Mckenna, F., Scott, M.H., and Fenves, G.L. (2006), OpenSees command language manual, Pacific Earthquake Engineering Research Center: California.

Nanda, S., Arthur, I., Sivakumar, V., Donohue, S., Bradshaw, A., Keltai, R., ... & Glynn, D. (2017). Monopiles subjected to uni-and multi-lateral cyclic loading. *Proceedings of the Institution of Civil Engineers-Geotechnical Engineering*, *170*(3), 246-258. https://doi.org/10.1680/jgeen.16.00110.

Poulos, H. G. (1982). Single pile response to cyclic lateral load. *Journal of the Geotechnical Engineering Division*, *108(3),* 355–375.

Rudolph, C., Bienen, B., & Grabe, J. (2014). Effect of variation of the loading direction on the displacement accumulation of large-diameter piles under cyclic lateral loading in sand. *Canadian geotechnical journal*, *51*(10), 1196-1206.

Wood, D. M. (2004). *Geotechnical modelling*. Spon Press, 504.

Yang, Z., and Elgamal, A. (2003). Application of unconstrained optimization and sensitivity analysis to calibration of a soil constitutive model. *International journal for numerical and analytical methods in geomechanics*, *27*(15), 1277-1297. https://doi.org/10.1002/nag.320

Yang, Z., Elgamal, A., and Parra, E. (2003). Computational model for cyclic mobility and associated shear deformation. *Journal of Geotechnical and Geoenvironmental Engineering*, *129*(12), 1119-1127. https://doi.org/10.1061/(ASCE)1090-0241(2003)129:12(1119)